Constraints on Thermal History of Mars From Depth of Pore Closure Below InSight

Szilárd Gyalay, Francis Nimmo, Ana-catalina Plesa, Mark Wieczorek

Geophysical Research Letters

RESEARCH LETTER
10.1029/2020GL088653

Special Section:
InSight at Mars

Constraints on Thermal History of Mars From Depth of Pore Closure Below InSight

Szilárd Gyalay[1], Francis Nimmo[1], Ana-Catalina Plesa[2], and Mark Wieczorek[3]

[1]Earth and Planetary Sciences, University of California, Santa Cruz, Santa Cruz, CA, USA, [2]German Aerospace Center (DLR), Cologne, Germany, [3]Observatoire de la Cote d'Azur, Nice, France

Key Points:

- The depth of porosity in Mars's crust depends most on the maximum heat flux after pore generation
- A seismic discontinuity at a depth of 8–11 km, as suggested by InSight, could be interpreted as the depth of porosity in the crust
- If pores closed at 8–11 km depth, it indicates pores formed prior to 4 Ga when heat flow was at least 60 mW m^{-2}

Correspondence to:
S. Gyalay,
sgyalay@ucsc.edu

Citation:
Gyalay, S., Nimmo, F., Plesa, A.-C., & Wieczorek, M. (2020). Constraints on thermal history of Mars from depth of pore closure below InSight. *Geophysical Research Letters*, *47*, e2020GL088653. https://doi.org/10.1029/2020GL088653

Received 29 APR 2020
Accepted 21 JUL 2020
Accepted article online 29 JUL 2020

Abstract Planetary crusts undergo viscous closure of pores at depth; if the thickness of this porous layer can be measured, constraints on crustal thermal evolution can be derived. We apply a pore closure model developed for the Moon to Mars and take into account the geological processes that may alter the depth of this transition region. If the 8–11 km deep discontinuity in seismic wave speed detected by the InSight lander marks the base of the porous layer, the heat flux at the time the porosity was created must have exceed 60 mW m^{-2}, probably indicating a time prior to 4 Ga.

Plain Language Summary On long timescales, and with enough heat or pressure, rocks in the crust of a planet can flow. This viscous deformation allows the empty pore spaces in a rock to close up. The history of the temperature at depth plays an important role in how deep one may expect porosity to exist. One can use a computational model to calculate the thickness of this porous layer as a function of the crust's thermal history. If the InSight Mars lander detects the thickness of such a porous layer, we can estimate the necessary temperature structure of the Martian crust and when porosity in the crust was generated. From a potential measurement of this porous layer at around 10 km thick, we predict the last significant pore formation event to have occurred at least 4 Gyr before present.

1. Introduction

The porosity structure of the Martian crust is important for several reasons. It controls the crustal water-carrying capacity (e.g., Clifford, 1993) and affects its near-surface thermal structure (Parmentier & Zuber, 2007). Furthermore, the porosity is an indication of the geological processes that have affected the crust, such as impact cratering, volcanism, and the emplacement of sediments. Less obviously, it contains a record of the thermal evolution of Mars, modulated by the history of crustal growth. Pores can close via plastic/viscous flow at a rate that is highly dependent on temperature (Hanna & Phillips, 2005); accordingly, if the depth to the base of the porous region can be established, the corresponding thermal structure may be deduced.

On the Moon, the presence of a porous layer roughly 40–85 km thick was identified using the very high resolution gravity data provided by GRAIL (Besserer et al., 2014; Wieczorek et al., 2013). The depth to the base of this layer was found to be consistent with models of viscous pore closure using simple lunar temperature structures (Wieczorek et al., 2013). In regions where the total crustal thickness is less than the depth of pore closure, the uppermost mantle also likely maintains porosity (Wieczorek et al., 2013). Thermally driven pore closure has also been modeled on icy satellites (e.g., Besserer et al., 2013; Eluszkiewicz, 2004; Kossacki & Lorenz, 1996) and on asteroids (e.g., Gail et al., 2015; Neumann et al., 2015). On the Moon, production of deep porosity was undoubtedly dominated by large impacts early in its history, and we will assume that the same is true for Mars.

Some studies of Martian aquifers (Clifford, 1993; Clifford & Parker, 2001) modeled porosity in Mars's crust as an exponential decay, scaled from a relationship hypothesized for the Moon, and observed in some geologic environments on Earth (e.g., Schmoker & Gautier, 1988). These relations focused on an elastic closure of pore space. At higher pressures or temperatures, rock deforms via ductile creep (Wong & Baud, 2012). On Earth, Manning and Ingebritsen (1999) interpret a drop in permeability at ~12 km depth due to ductile creep closing pores. Because of the lower gravity (and thus reduced elastic closure) on the Moon and Mars in conjunction with high heating early in their history, it is the latter process which we focus on in this work.

On the Moon, an apparent decay in seismic scattering with depth has been used to infer the depth to which fractured rocks extend (Gillet et al., 2017). In a similar fashion, the recent emplacement of the InSight seismometer on the Martian surface provides the possibility of measuring the thickness of the porous layer. In this work, we carry out simple models of viscous pore closure for the Martian crust and show how the thickness of the porous layer can be related to the peak heat flux experienced. In section 2, we review the mathematics of viscous pore closure. In section 3, we investigate the potential confounding effects of geological processes of Mars's crust. In section 4 we use a detected seismic discontinuity beneath InSight to quantify the thermal environment at the landing site when pore formation stopped, and thus determine when it stopped. We conclude with section 5.

2. Viscous Closure of Pores on Mars

We approach the problem in a similar fashion to Wieczorek et al. (2013), and references therein (i.e., Eluszkiewicz, 2004; Fowler, 1985; Nimmo et al., 2003). How quickly the porosity ϕ closes over time t depends on the dynamic viscosity of the materials η and the overburden pressure P:

$$\frac{\partial \phi}{\partial t} = -\phi \frac{P}{\eta}. \tag{1}$$

Pressure $P = \rho g z$, where ρ is crustal density, g is gravitational acceleration, and z is depth in the crust.

Under high pressures, viscosity does not depend on grain size but does depend on stress σ, rheological constants A and n, an activation energy Q, and the gas constant R:

$$\eta = \frac{\sigma^{1-n}}{A} \exp\left(\frac{Q}{RT}\right). \tag{2}$$

We take this stress to be equal to the overburden pressure, $\sigma = P$. In reality there is a constant of proportionality of order unity in Equation 2 depending on the relationship of overburden pressure to the deviatoric stress, and the ratio of initial to current porosity (e.g., Eluszkiewicz, 2004). However, since the heat flux necessary for pore closure ultimately depends on the logarithm of P (section 2.3), neglecting this constant does not introduce significant errors. For instance, substituting $\sigma = 0.1P$ instead of $\sigma = P$ in Equation 2 depresses the depth of pore closure by ~2 km.

2.1. Constant Heat Flux Case

For the case of constant temperature, we solve Equation 1 to find ϕ relative to some initial porosity ϕ_0 after some elapsed time t as

$$\phi = \phi_0 \exp\left(\frac{-Pt}{\eta}\right). \tag{3}$$

For an initially porous crust, we can use this equation to calculate how much the porosity at each depth has changed as a function of time. We assume pores have effectively closed when they reach a critical porosity that is a factor of e^2 less than the initial. The depth of the porous layer after some time is then limited by where porosity is still present; because of the strong temperature dependence of viscosity, the transition to pore-free material is typically abrupt (less than a few km; Figure 1a). Because this transition is abrupt, the exact pore closure criterion matters very little: one can take the characteristic criterion to be a factor of e or 10 and achieve nearly identical results.

For our nominal model, we use a gravitational acceleration of 3.7 m s^{-2}, an upper crustal density of 2,800 kg m^{-3}, a rock thermal conductivity of 3.0 W m^{-1} K^{-1}, no crustal heat production, and a constant surface temperature of 250 K. In this investigation we model Mars with both wet and dry diabase (as used in previous investigations of Mars, see, e.g., Hanna & Phillips, 2005). For wet diabase, $Q = 276 \pm 14$ kJ Mol^{-1}, $n = 3.05 \pm 0.15$, and $A = 6.12 \pm 3.06 \cdot 10^{-2}$ MPa^{-n} s^{-1} (Caristan, 1980). Caristan (1980) did not include exact uncertainties, but noted that uncertainty in Q and n would not exceed 5%, and A could vary by a factor of 2. For dry diabase, $Q = 485 \pm 30$ kJ Mol^{-1}, $n = 4.7 \pm 0.6$, and $A = 1.9 \pm 1.1 \cdot 10^{2}$ MPa^{-n} s^{-1}

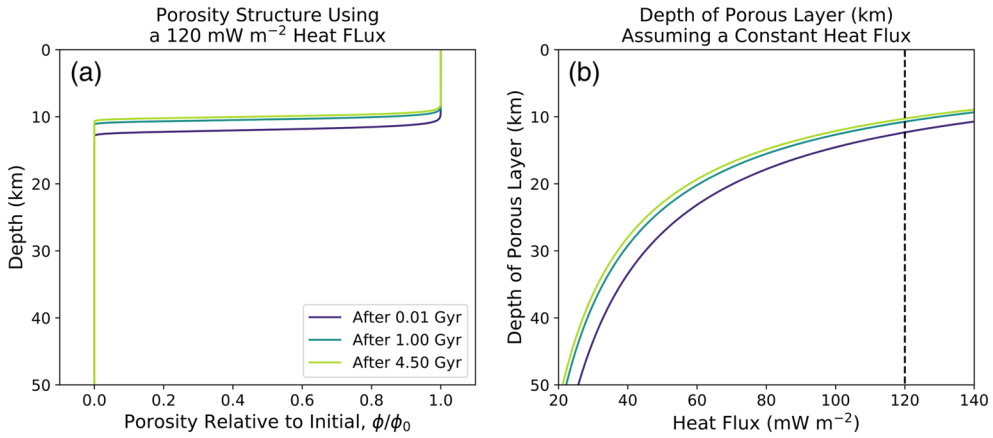

Figure 1. Panel (a) Porosity structure after 10 Myr, 1 Gyr, and 4.5 Gyr for an assumed heat flux of 120 mW m^{-2}. Temperature structure at depth is calculated from Fourier's law of thermal conduction for a surface temperature of 250 K, a thermal conductivity of 3 W m^{-1} K^{-1} and no crustal heat production. We use the rock rheology of wet diabase from Caristan (1980) without consideration for uncertainty. Porosity decreases from its initial value to 0 over a sharp interval of about 2 km. Panel (b) Depth of pore closure (where the porosity is reduced by a factor e^2 with respect to the initial value) as a function of heat flux. The dashed line illustrates the heat flux used for (a).

(Mackwell et al., 1998). Some other parameter values are uncertain; in particular, thermal conductivity has a strong dependence on porosity as well as the contents of its pore space. We discuss the effect of these uncertainties further below and in Appendix A.

For the purpose of illustration, we assume a single rheology (wet diabase) and plot how the depth of pore closure changes through time for a range of constant heat fluxes in Figure 1b. Most pore closure happens in a short time span. The depth of pore closure over the age of the solar system, as shown in Figure 1b, is highly dependent on the assumed heat flux, ranging from depths of more than 50 km for low heat fluxes of about 20 mW m^{-2} to about 10 km for heat fluxes in excess of 120 mW m^{-2}. Present-day heat fluxes on Mars are expected to be roughly 20 mW m^{-2} (see below), but would have been higher at earlier times. It is thus important to take into account the time evolution of heat flux.

2.2. Decreasing Heat Flux Case

To investigate the effect of a changing heat flux, we make use of a suite of thermal evolution models developed by Plesa et al. (2018). The model uses a fully 3-D geometry to model the thermal evolution and interior dynamics of Mars. We focus on their case 110, as it represents an upper bound in terms of heat flux through time. Similar to most other cases of Plesa et al. (2018), case 110 uses a crustal thermal conductivity of 3 W m^{-1} K^{-1}, latitudinal variations of the surface temperature leading to a surface temperature of 235 K at InSight location (Kieffer, 2013; Ohring & Mariano, 1968), and spatial variations of crustal thickness. The average crustal thickness of this model is 45 km and the crustal heat production rate is 20% higher than the value suggested by GRS (Hahn et al., 2011). The crustal heat production for case 110 decreases exponentially from an initial value of 331.1 pW kg^{-1}. We note that this case matches available geophysical, geological, and petrological constraints (cf. supporting information of Plesa et al., 2018). We use Equation 1 to evolve the porosity forward in time, taking into account the effect of the changing crustal temperature structure on the viscosity via Equation 2. Figure 2a shows the model surface heat flux through Martian history.

We begin the porosity evolution calculation at different points in Mars's history. In this model, porosity is assumed to be present in the crust at some time t_0, and then we compute the depth of pore closure. For each starting time point, we evolved Equation 1 forward in time over either 10 Myr or 1 Gyr, showing that the results are not sensitive to the total elapsed time after initation of pore closure (Figure 2b). Pore closure reaches shallower depths in cases when closure started earlier (when temperatures were higher). Because of the continuing decrease in heat flux, the pore closure depth is much more sensitive to the heat flux at the start of pore closure than on the total duration of closure. In effect, the present-day depth of pore closure is a "fossil" signature of an ancient heat flux. We accordingly are justified in using an analytical approach in which the initial, maximum heat flux is calculated from the present-day depth of pore closure.

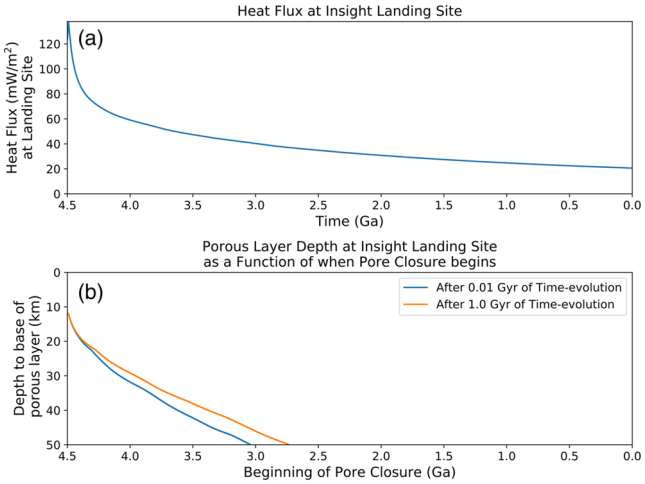

Figure 2. Panel (a) Surface heat flux at InSight's landing site, modeled through Martian history. This particular model is case 110 from Plesa et al. (2018) and uses a thermal conductivity $k = 3\ \mathrm{W\ m^{-1}\ K^{-1}}$. The surface temperature in this Plesa et al. (2018) model was 235 K at the InSight landing site. Crustal heat production was initially 331.1 pW $\mathrm{kg^{-1}}$ and decreased exponentially to 59 pW $\mathrm{kg^{-1}}$. Panel (b) To account for how a changing heat flux affects pore closure, we can no longer use Equation 3 over the total elapsed time. However, we may still employ this equation over short and successive time steps (we use 100 kyr). For example, if we begin pore closure at 4 Ga, we first assume the heat flux indicated in panel (a) for 4 Ga (~60 mW $\mathrm{m^{-2}}$) and find porosity as a function of depth with Equations 2 and 3 after 100 kyr have elapsed. For the next time step, we use the heat flux 100 kyr after our start time and repeat the process. After the necessary number of time steps, we calculate the depth of the porous layer after 10 Myr and 1 Gyr of evolution from the corresponding start time. Due to the uncertainty in when pore generation may have ended, we allow the beginning of pore closure to vary from 1.0–4.5 Ga. So as a function of this start time, we plot the depth of the porous layer after 10 Myr (blue line) and 1 Gyr (orange line) of heat flux evolution. We use the rock rheology of wet diabase from Caristan (1980). While porosity could continue into the upper mantle (cf. Wieczorek et al., 2013), we are primarily concerned with pore closure in the crust, as InSight has potentially detected pore closure at only ~10 km depth (Lognonné et al., 2020). As such, we truncate results at depths greater than a generous crustal thickness of 50 km.

2.3. Necessary/Maximum Heat Flux as a Function of Pore Closure Depth

Assume that pores close at a critical porosity ϕ_C (we use $\phi_C = e^{-2}\phi_0$). Rearranging Equation 3, the critical temperature T_C to close pores at some depth $z = (P/\rho g)$ (we account for uncertainty in the density due to porosity in Appendix A) after some time t is

$$T_C = \frac{Q/R}{\ln\left(\frac{tP^nA}{\ln(\phi_0/\phi_C)}\right)}. \tag{4}$$

This expression shows that the closure temperature is strongly dependent on the activation energy Q and weakly dependent on the overburden pressure P and elapsed time t.

The temperature at depth is related to heat flux by Fourier's law of thermal conduction. We can thus determine the surface heat flux necessary to close pores at a certain depth:

$$F_C = \frac{k}{z}\left[\frac{Q/R}{\ln\left(\frac{tP^nA}{\ln(\phi_0/\phi_C)}\right)} - T_S + \frac{\rho H z^2}{2k}\right], \tag{5}$$

where T_S is the surface temperature, and H is the crustal heat production rate per unit mass. Because a decreasing heat flux results in little change in the depth of pore closure over time (assuming that no additional porosity is being generated, see Figure 2b), we can use a small elapsed time such as $t = 10$ Myr and be confident that this results in the maximum heat flux a region can have experienced in its history.

3. Effects of Geology

Until now, we have made several simplifying assumptions in this analysis. We assumed pores close only viscously and neglected other ways of closing porosity such as cementation or volcanism. We also assume that the entire crust is initially porous and that no new porosity is generated. Nonetheless, any subsurface region in which porosity is maintained can never have exceeded a given temperature since the most recent generation of porosity, placing an upper bound on the heat flux. For the Moon, it is thought that early bombardment was the main source of porosity and that the decline in impacts greatly reduced subsequent pore generation (Wahl et al., 2020; Wieczorek et al., 2013). On Mars, the last events to generate significant porosity were likely the impacts that formed the Borealis Basin (>4.47 Ga) or Hellas, Isidis, and Argyre basins (~3.8–4.1 Ga) (Bottke & Andrews-Hanna, 2017).

In this section, we explore the regional geology near InSight and how it may affect our analysis. InSight landed in Elysium Planitia near the boundary of Mars's crustal dichotomy. From orbital data, InSight appears to have landed on a plain of early-Amazonian or late-Hesperian (~3.0 Ga) lava flows 200–300 m thick, which overlie sedimentary rocks of Noachian age (~3.7–4.1 Ga) (Pan et al., 2020). The sediments themselves may overlie altered basaltic rocks that are compacted at depth (Smrekar et al., 2019). The surface geology at the landing site was well-predicted by the orbital data (Golombek et al., 2020). Initial analyses of the InSight seismic data using a seismic receiver function analysis shows that there is a seismic discontinuity at 8–11 km depth (Lognonné et al., 2020). This discontinuity occurs within the crust of Mars, and potentially indicates the presence of altered/fractured rocks to that depth (Lognonné et al., 2020).

We consider four geological phenomena that may affect the depth of pore closure beneath the InSight landing site: sediment accumulation, emplacement of lava flows, erosion, and the presence of groundwater. If

sedimentation occurred after maximum heating, the extra overburden pressure it applies at depth would not cause additional compaction but may effectively increase the depth to pore closure by the thickness of the additional sediment. In addition, the sediments themselves would be expected to form with significant porosity (see Lewis et al., 2019). Lava flows would greatly increase the surface temperature, but the thermal anomaly will only propagate downwards to a depth comparable to the flow thickness, which is likely much less than the porous layer depth. Like sediment layers, this layer of lava would also increase the depth to pore closure by the thickness of the deposit, and the lava flows would likely also contain some porosity (e.g., Rust et al., 1999, and references therein). Erosion would remove at least some of the upper portion of the porous layer. However, there is little evidence for large-scale erosive events in this region of Mars.

The presence of pore water will change the deviatoric stress. However, because of the large density contrast between water and rock, and the logarithmic dependence on P (Equation 5), this effect is negligible. Groundwater can also aqueously alter the mineralogy via diagenesis (see section 4 below). Most importantly for our study, an aquifer can affect the temperature structure of the crust and thus the depth to which pores close. The presence of liquid water in the pore space of Martian rock can lower the effective thermal conductivity of the rock (e.g., Hanna & Phillips, 2005)—increasing the thermal gradient and thus reducing the thickness of the porous layer. The thermal conductivity of the Martian crust may be somewhere between 2 and 3 $\mathrm{W\,m^{-1}\,K^{-1}}$ (e.g., Clauser & Huenges, 1995; Seipold, 1998) while water's thermal conductivity is 0.57 $\mathrm{W\,m^{-1}\,K^{-1}}$ (Demming, 2002). A similar reduction in conductivity will arise if the pores are empty rather than water filled. Uncertainty in the thermal conductivity has the largest effect on the uncertainty in the calculated maximum heat flux (see Appendix A).

Another possibility to consider is if water in the pore space of the Martian crust is undergoing convection. This is important because convection decreases the thermal gradient—making the required heat flux to close pores at a given depth under the assumption of conduction (Equation 5) an underestimate. We can calculate whether the fluid would convect using the Rayleigh number for a fluid in a porous medium:

$$Ra = \frac{\rho_w \alpha_w \Delta T g K l}{\phi \eta_w \kappa_w}, \tag{6}$$

where ρ_w is the density of water, α_w is the thermal expansivity of water, ΔT is the temperature difference across the change in depth, K is the permeability of the Martian regolith, l is the length scale, ϕ is the porosity of the regolith, η_w is the viscosity of the water, and κ_w is the thermal diffusivity of water (Hewitt et al., 2014).

Although most of these variables are approximately known, the permeability and porosity of the crust are very uncertain. Hanna and Phillips (2005) estimated the vertical extent of potential Noachian aquifers by modeling the closure of pores in a manner resembling our approach. We approximate from their results, which derived a porosity that varied from 0.16 at the surface to 0.04 at a depth of ~10 km. They predicted the permeability of Martian regolith to vary from 10^{-11} $\mathrm{m^2}$ at the surface to 10^{-15} $\mathrm{m^2}$ at depths of 5 km or more.

Taking an order of magnitude approach, we take $\rho_w = 10^3$ $\mathrm{kg\,m^{-3}}$, $\alpha_w = 10^{-4}$ $\mathrm{K^{-1}}$, $g = 4$ $\mathrm{m\,s^{-2}}$, $\eta_w = 10^{-3}$ Pa s, and $\kappa_w = 10^{-7}$ $\mathrm{m^2\,s^{-1}}$. If we take a length scale of 10 km, then let us take $K = 10^{-14}$ $\mathrm{m^2}$ as a rough geometric mean of permeability (weighted more toward 10^{-15} $\mathrm{m^2}$ as half the depth has that permeability). Similarly, let us assume a mean porosity of 0.1. If the surface of Mars is near the freezing temperature of water, then we may take $\Delta T = 100$ K as an upper bound. The Rayleigh number is then ~400. We do not expect any flow below a Rayleigh number of $4\pi^2$, and then some transition range above that (Hewitt et al., 2014). Depending on alterations in our order-of-magnitude assumptions, our simplified aquifer may be transitioning into convection. Since the effect of any such convection is to reduce the temperature gradient, our conductive solutions for the heat flux required to produce a particular porous layer depth (see below) will, if anything, be underestimates.

4. Application to InSight's Landing Site

InSight has detected a discontinuity in seismic wave velocity 8–11 km below the surface, which may indicate the presence of altered or fractured rocks to that depth (Lognonné et al., 2020). We treat this as the transition from porous to compacted crust, but as a deeper probing of the Martian crust requires higher-magnitude

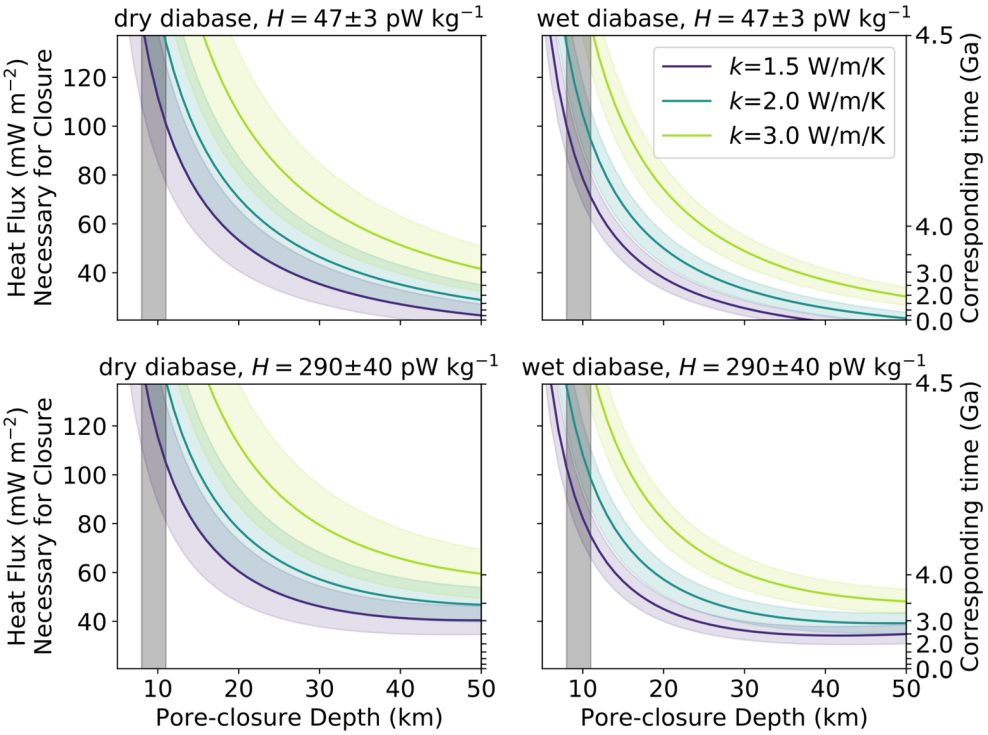

Figure 3. For each rheology and crustal heat production (H) combination, we vary the thermal conductivity to find the necessary surface heat flux needed to close pores viscously as a function of depth (Equation 5), assuming 10 Myr have elapsed to close pores. The secondary y axis relates the necessary heat flux to the time that heat flux occurred at the InSight landing site according to case 110 of the Plesa et al. (2018) Mars thermal evolution model. The colored shaded regions highlight the corresponding uncertainty for each assumed thermal conductivity. Examining multiple thermal conductivities allows us to ascertain its effect on the maximum heat flux without needing to factor it into the calculation of uncertainty. The vertical gray-shaded region highlights the 8–11 km depth at which InSight detects a discontinuity in seismic wave speed.

marsquakes, we cannot yet be sure if porosity actually continues to greater depths. Mineralogical changes can also cause seismic discontinuities, but the two transitions need not be independent: fluids fluxing through the permeable crust may cause diagenesis (e.g., Sun et al., 2019) and a corresponding reduction in seismic velocities, while leaving the impermeable crust unchanged. In effect, the porous/compacted rock boundary can become a mineralogical boundary that is detectable by InSight. In any event, if a different depth of pore closure is ultimately detected, we can deduce the maximum heat flux experienced at the InSight landing site after pore generation.

In making our prediction for maximum heat flux experienced at the InSight landing site, we account for the uncertainty of each term in Equation 5 (see Appendix A). To account for a wide range of estimates of thermal conductivity of the Martian crust (with or without groundwater), we use separate thermal conductivities of $k = 1.5$, 2.0, and 3.0 W m^{-1} K^{-1}. We use an average present-day temperature of 235 K at the InSight landing site (Plesa et al., 2018). Solar luminosity in the early solar system was as little as 70% of its present value (Ribas, 2010). To account for this range, we use a surface temperature $T_S = 220 \pm 30$ K. We use a crustal density $\rho = 2{,}950 \pm 250$ kg m^{-3}, and the rheological constants as listed in section 2.1. For each rheology and thermal conductivity, we calculate the necessary heat flux (and its uncertainty) for pore closure as a function of pore closure depth. We assume two extremes of crustal heat production: that of the present day (47 ± 3 pW kg^{-1}) and what one might expect of Mars in its earliest days (290 ± 40 pW kg^{-1}) (Hahn et al., 2011; Plesa et al., 2018). Results are displayed in Figure 3.

As expected, higher heat fluxes, lower thermal conductivities, or weaker rheologies result in thinner porous layers. For the same given temperature required to close pores at some depth, a higher crustal heat production will result in a higher surface heat flux. In turn, this heat flux can be related to a particular time in

Martian history. For example, to close pores at a depth of 8–11 km requires heat fluxes in excess of 60 mW m^{-2} for a wet diabase rheology. For dry diabase, the heat fluxes are larger. A larger crustal heat production (as one would expect early in Mars's history) will result in a higher surface heat flux when pores closed, but the effect is not significant when closing pores at shallower depths. Based on the surface heat flux through time resulting from the thermal evolution model of Plesa et al. (2018) plotted in Figure 2a, we conclude that pore closure must have occurred before 4 Ga and that pore production must have been even earlier. This conclusion is robust to uncertainties in thermal conductivity, rheology, and crustal heat production (at least to close pores at ~10 km depth). Because the employed thermal evolution model of Plesa et al. (2018) is an upper bound on likely heat fluxes, this age estimate is conservative and robust to uncertainties in Mars's initial conditions: Other cases cool to a heat flux of 60 mW m^{-2} earlier in Mars's history.

Our constraint can be compared with thermal models and other measurements. For instance, Hauck and Phillips's (2002) thermal model predicts a surface heat flux of up to ~65 mW m^{-2} before 4 Ga, albeit for an average crustal thickness of 62 km. By examining the viscous relaxation of craters, Karimi et al. (2016) were able to construct a map of Mars's surface heat flux during the Noachian, finding a heat flux ~70 mW m^{-2} near where InSight landed. Both Hauck and Phillips's (2002) thermal model and Karimi et al.'s (2016) inversion are consistent with heat fluxes exceeding 60 mW m^{-2} before 4 Ga. Another independent estimate of paleo heat fluxes may be derived from measurements of elastic thickness. For instance, McGovern et al. (2004) find heat fluxes in excess of 35, 43, 48, and 50 mW m^{-2} for four Noachian terrains. Likewise, Broquet and Wieczorek (2019) generally obtain heat fluxes greater than 50 mW m^{-2} for ancient, eroded volcanoes. Although uncertain, all these estimates are very consistent with our constraint.

5. Conclusion

This analysis assumes that the porous-to-nonporous transition is the cause of the seismic wave speed discontinuity detected by InSight (Lognonné et al., 2020). From that transition depth we conclude that pores formed prior to 4 Ga and in the presence of a heat flux exceeding 60 mW m^{-2}. If the seismic discontinuity instead marks a different transition of rock composition and porosity continues to a greater depth, this may indicate a delayed onset of pore closure until later in Mars's history when it had cooled down. Alternatively, a Mars that had started off colder would also ensure a smaller heat flux, resulting in a deeper porous-to-compacted transition. Finally, if the crust has cooled significantly, additional layers of sediments or lavas could depress the transition from porous-to-compacted crust without further closing pores due to the extra overburden pressure.

In the future, further seismic events will allow improved estimation of the depth at which pores close. When such a new measurement is made, the approach we present in this paper can be used to further clarify the thermal state of the ancient Martian crust.

Appendix A: Quantifying Uncertainty

Equation 5 allows us to determine the maximum heat flux a region experienced as a function of the depth to pore closure in the crust. However, it also relies on assumptions of the rock types that make up the crust, the rheological constants for each rock type, surface temperature, rock density, thermal conductivity of the rock, and heat production within the rock.

One can find the uncertainty in maximum heat flux as a function of the uncertainties of each variable:

$$\begin{aligned}\delta F_C^2 &= \left(\frac{\partial F_C}{\partial k}\right)^2 \delta k^2 + \left(\frac{\partial F_C}{\partial T_S}\right)^2 \delta T_S^2 + \left(\frac{\partial F_C}{\partial Q}\right)^2 \delta Q^2 + \left(\frac{\partial F_C}{\partial H}\right)^2 \delta H^2 \\ &+ \left(\frac{\partial F_C}{\partial A}\right)^2 \delta A^2 + \left(\frac{\partial F_C}{\partial \rho}\right)^2 \delta \rho^2 + \left(\frac{\partial F_C}{\partial n}\right)^2 \delta n^2.\end{aligned} \tag{A1}$$

Taking each partial derivative of Equation 5 and inserting it into Equation A1, we find the uncertainty to be

$$\delta F_C^2 = F_C^2\left(\frac{\delta k}{k}\right)^2 + \left(\frac{k}{z}\right)^2 \delta T_S^2 + \left(F_C + \frac{kT_S}{z}\right)^2 \left(\frac{\delta Q}{Q}\right)^2 + \left(\frac{\rho z}{2}\right)^2 \delta H^2 + \frac{\left(F_C + \frac{kT_S}{z} - \frac{\rho H z}{2}\right)^2}{\ln\left(\frac{tP^n A}{\ln(\phi_0/\phi_C)}\right)^2}\left[\left(\frac{\delta A}{A}\right)^2 + \left(\frac{n}{\rho} + \frac{Hz}{2}\right)^2 \delta\rho^2 + \ln(P)^2 \delta n^2\right]. \quad \text{(A2)}$$

By inspecting Equation A2, one can see that the variables whose individual uncertainties have the largest effect upon the total uncertainty are the thermal conductivity k, the surface temperature T_S, and the activation energy Q.

Data Availability Statements

Data for the heat flux and temperature as a function of depth of the Martian crust were outputs of the Plesa et al. (2018) 3-D Mars thermal evolution model at the InSight landing site. Data for several cases (the conditions of each are detailed in the supporting information of Plesa et al., 2018) are archived in the Dryad repository at https://doi.org/10.7291/D1467K.

Acknowledgments
We thank Adrien Broquet for his insightful comments on our manuscript. We also thank Walter Kiefer and an anonymous reviewer for their thoughtful and constructive comments. This is InSight contribution number 163. Parts of this work were supported by NASA Grant 80NSSC18K1627 to F. N. A.-C. P. gratefully acknowledges the financial support and endorsement from the DLR Management Board Young Research Group Leader Program and the Executive Board Member for Space Research and Technology. M. A. W. was supported by the French Space Agency (CNES).

References

Besserer, J., Nimmo, F., Roberts, J. H., & Pappalardo, R. T. (2013). Convection-driven compaction as a possible origin of Enceladus's long wavelength topography. *Journal of Geophysical Research: Planets*, *118*, 908–915. https://doi.org/10.1002/jgre.20079

Besserer, J., Nimmo, F., Wieczorek, M. A., Weber, R. C., Kiefer, W. S., McGovern, P. J., et al. (2014). GRAIL gravity constraints on the vertical and lateral density structure of the lunar crust. *Geophysical Research Letters*, *41*, 5771–5777. https://doi.org/10.1002/2014GL060240

Bottke, W. F., & Andrews-Hanna, J. C. (2017). A post-accretionary lull in large impacts on early Mars. *Nature Geoscience*, *10*, 344348. https://doi.org/10.1038/ngeo2937

Broquet, A., & Wieczorek, M. (2019). The gravitational signature of Martian volcanoes. *Journal of Geophysical Research: Planets*, *124*, 2054–2086. https://doi.org/10.1029/2019JE005959

Caristan, Y. (1980). High temperature mechanical behavior of Maryland diabase (Unpublished doctoral dissertation).

Clauser, C., & Huenges, E. (1995). Thermal Conductivity of Rocks and Minerals. In T. Ahrens (Ed.), *Rock Physics & Phase Relations: A Handbook of Physical Constants* (Vol. 3, pp. 105–127). Washington, DC: American Geophysical Union. https://doi.org/10.1029/RF003p0105

Clifford, S. M. (1993). A model for the hydrologic and climatic behavior of water on Mars. *Journal of Geophysical Research*, *98*(E6), 10973. https://doi.org/10.1029/93JE00225

Clifford, S. M., & Parker, T. J. (2001). The evolution of the Martian hydrosphere: Implications for the fate of a primordial ocean and the current state of the northern plains. *Icarus*, *154*(1), 40–79. https://doi.org/10.1006/icar.2001.6671

Demming, D. (2002). *Introduction to Hydrology*. New York: McGraw-Hill.

Eluszkiewicz, J. (2004). Compaction and internal structure of Mimas. *Icarus*, *84*(1), 215. https://doi.org/10.1016/0019-1035(90)90167-8

Fowler, A. C. (1985). A mathematical model of magma transport in the asthenosphere. *Geophysical & Astrophysical Fluid Dynamics*, *33*(1–4), 63. https://doi.org/10.1080/03091928508245423

Gail, H.-P., Henke, S., & Trieloff, M. (2015). Thermal evolution and sintering of chondritic planetesimals II. Improved treatment of the compaction process. *Astronomy & Astrophysics*, *576*(A60), 1–19. https://doi.org/10.1051/0004-6361/201424278

Gillet, K. M., Calvet, M., & Monnereau, M. (2017). Scattering attenuation profile of the moon: Implications for shallow moonquakes and the structure of the megaregolith. *Physics of the Earth and Planetary Interiors*, *262*, 28. https://doi.org/10.1016/j.pepi.2016.11.001

Golombek, M., Warner, N. H., Grant, J. A., Hauber, E., Ansan, V., Weitz, C. M., et al. (2020). Geology of the insight landing site on Mars. *Nature Communications*, *11*, 1014. https://doi.org/10.1038/s41467-020-14679-1

Hahn, B. C., McLennan, S. M., & Klein, E. C. (2011). Martian surface heat production and crustal heat flow from Mars Odyssey gammaray spectrometry. *Geophysical Research Letters*, *38*, L14203. https://doi.org/10.1029/2011GL047435

Hanna, J. C., & Phillips, R. J. (2005). Hydrological modeling of the Martian crust with application to the pressurization of aquifers. *Journal of Geophysical Research*, *110*, E01004. https://doi.org/10.1029/2004JE002330

Hauck, S. A., & Phillips, R. J. (2002). Thermal and crustal evolution of Mars. *Journal of Geophysical Research*, *107*(E7), 6–1–6–19. https://doi.org/10.1029/2001JE001801

Hewitt, D. R., Neufeld, J. A., & Lister, J. R. (2014). High Rayleigh number convection in a three-dimensional porous medium. *Journal of Fluid Mechanics*, *748*, 879. https://doi.org/10.1017/jfm.2014.216

Karimi, S., Dombard, A. J., Buczkowski, D. L., Robbins, S. J., & Williams, R. M. (2016). Using the viscoelastic relaxation of large impact craters to study the thermal history of Mars. *Icarus*, *272*, 102–113. https://doi.org/10.1016/j.icarus.2016.02.037

Kieffer, H. H. (2013). Thermal model for analysis of Mars infrared mapping. *Journal of Geophysical Research: Planets*, *118*, 451–470. https://doi.org/10.1029/2012JE004164

Kossacki, K. J., & Lorenz, R. D. (1996). Hiding Titan's ocean: Densification and hydrocarbon storage in an icy regolith. *Planetary and Space Science*, *44*(9), 1029.

Lewis, K. W., Peters, S., Gonter, K., Morrison, S., Schmerr, N., Vasavada, A., & Gabriel, T. (2019). A surface gravity traverse on Mars indicates low bedrock density at Gale crater. *Science*, *363*(6426), 535–537. https://doi.org/10.1126/science.aat0738

Lognonné, P., Banerdt, W. B., Pike, W. T., Giardini, D., Christensen, U., Garcia, R. F., et al. (2020). Constraints on the shallow elastic and anelastic structure of mars from insight seismic data. *Nature Geoscience*, *13*, 213. https://doi.org/10.1038/s41561-020-0536-y

Mackwell, S. J., Zimmerman, M. E., & Kohlstedt, D. L. (1998). High-temperature deformation of dry diabase with application to tectonics on Venus. *Journal of Geophysical Research*, *103*(B1), 975–984. https://doi.org/10.1029/97JB0267

Manning, C. E., & Ingebritsen, S. E. (1999). Permeability of the continental crust: Implications of geothermal data and metamorphic systems. *Reviews of Geophysics*, *37*(1), 127–150. https://doi.org/10.1029/1998RG900002

McGovern, P. J., Solomon, S. C., Smith, D. E., Zuber, M. T., Simons, M., Wieczorek, M. A., et al. (2004). Correction to "localized gravity/topography admittance and correlation spectra on Mars: Implications for regional and global evolution". *Journal of Geophysical Research*, *109*, E07007. https://doi.org/10.1029/2004JE002286

Neumann, W., Breuer, D., & Spohn, T. (2015). Modelling the internal structure of Ceres: Coupling of accretion with compaction by creep and implications for the water-rock differentiation. *Astronomy & Astrophysics*, *584*, A117. https://doi.org/10.1051/0004-6361/201527083

Nimmo, F., Pappalardo, R. T., & Giese, B. (2003). On the origins of band topography, Europa. *Icarus*, *166*(1), 21. https://doi.org/10.1016/j.icarus.2003.08.002

Ohring, G., & Mariano, J. (1968). Seasonal and latitudinal variations of the average surface temperature and vertical temperature profile on Mars. *Journal of the Atmospheric Sciences*, *25*(5), 673–681. https://doi.org/10.1175/1520-0469(1968)025<0673:SALVOT>2.0.CO;2

Pan, L., Quantin-Nataf, C., Tauzin, B., Michaut, C., Golombek, M., Lognonné, P., et al. (2020). Crust stratigraphy and heterogeneities of the first kilometers at the dichotomy boundary in western Elysium Planitia and implications for InSight lander. *Icarus*, *338*, 113511. https://doi.org/10.1016/j.icarus.2019.113511

Parmentier, E. M., & Zuber, M. T. (2007). Early evolution of Mars with mantle compositional stratification or hydrothermal crustal cooling. *Journal of Geophysical Research*, *112*, E02007. https://doi.org/10.1029/2005JE002626

Plesa, A.-C., Padovan, S., Tosi, N., Breuer, D., Grott, M., Wieczorek, M. A., et al. (2018). The thermal state and interior structure of Mars. *Geophysical Research Letters*, *45*, 12,198. https://doi.org/10.1029/2018GL080728

Ribas, I. (2010). The Sun and stars as the primary energy input in planetary atmospheres. *Proceedings of the International Astronomical Union*, *5*(S264), 3–18. https://doi.org/10.1017/S1743921309992298

Rust, A. C., Russel, J. K., & Knight, R. J. (1999). Dielectric constant as a predictor of porosity in dry volcanic rocks. *Journal of Volcanology and Geothermal Research*, *99*(1), 79–96. https://doi.org/10.1016/S0377-0273(99)00055-4

Schmoker, J. W., & Gautier, D. L. (1988). Sandstone porosity as a function of thermal maturity. *Geology*, *16*(11), 1007–1010. https://doi.org/10.1130/0091-7613(1988)016<1007:SPAAFO>2.3.CO;2

Seipold, U. (1998). Temperature dependence of thermal transport properties of crystalline rocks: A general law. *Tectonophysics*, *291*, 161. https://doi.org/10.1016/S0040-1951(98)00037-7

Smrekar, E. E., Lognonné, P., Spohn, T., Banerdt, W. B., Breuer, D., Christensen, U., et al. (2019). Pre-mission insights on the interior of Mars. *Space Science Reviews*, *215*, 3. https://doi.org/10.1007/s11214-018-0563-9

Sun, V. Z., Stack, K. M., Kah, L. C., Thompson, L., Fischer, W., Williams, A. J., et al. (2019). Late-stage diagenetic concretions in the Murray formation, Gale crater, Mars. *Icarus*, *321*, 866–890. https://doi.org/10.1016/j.icarus.2018.12.030

Wahl, D., Wieczorek, M. A., Wnnemann, K., & Oberst, J. (2020). Crustal porosity of lunar impact basins. *Journal of Geophysical Research: Planets*, *125*, e2019JE006335. https://doi.org/10.1029/2019JE006335

Wieczorek, M. A., Neumann, G. A., Nimmo, F., Kiefer, W. S., Taylor, G. J., Melosh, H. J., et al. (2013). The crust of the Moon as seen by GRAIL. *Science*, *339*(6120), 671–675. https://doi.org/10.1126/science.1231530

Wong, T.-F., & Baud, P. (2012). The brittle-ductile transition in porous rock: A review. *Journal of Structural Geology*, *44*, 25–53. https://doi.org/10.1016/j.jsg.2012.07.010